Ecography

ECOG-00975
Andrello, M., Nilsson Jacobi, M., Manel, S., Thuiller, W. and Mouillot, D. 2014. Extending networks of protected areas to optimize connectivity and population growth rate. – Ecography doi: 10.1111/ecog.00975

Supplementary material

Appendix 1

Here we give an example of application of the original EPT algorithm by (Nilsson Jacobi and Jonsson 2011) and highlight the importance of a spatially balanced choice of protected sites. This is achived by using the full spectrum of eigenvalues and not only the dominant eigenvalue.

Nilsson Jacobi and Jonsson (2011) showed that the contribution of a productivity increase in site *i* to the eigenvalues (mimicking protection at site *i*) can be found by the linear approximation:

$$\hat{\lambda}_k^{\text{new}} = \lambda_k \left(1 + \delta \mathbf{v}_{ki} \mathbf{u}_{ki}\right) \quad (1)$$

Here, λ_k is the k-th eigenvalue of the connectivity matrix, $\mathbf{u}_k$ and $\mathbf{v}_k$ are the right and left eigenvectors associated with λ_k and δ is the productivity increase in site *i*. The product between $\mathbf{v}_{k,i}\mathbf{u}_{k,i}$ is the donor-recipient value (Nilsson Jacobi and Jonsson 2011): it scales the productivity increase by the ability of a site to act both as a donor (left eigenvector) and a recipient (right eigenvector) of propagules. The product $\delta\mathbf{v}_{k,i}\mathbf{u}_{k,i}$ is the contribution of the productivity increase in site *i* to the k-th eigenvalue. The sites with the highest contributions are the most important for population persistence. A thorough demonstration of the importance of the donor-recipient value as measure of site contribution to population persistence and on the superiority of the donor-recipient metric relative to other metrics (local retention rates, source strength, sink strength) can be found in Nilsson Jacobi and Jonsson (2011).

Consider the population in **Figure A1(a),** composed of two nearly independent clusters and its connectivity matrix in **Table A1**.

The first cluster comprises sites 1 and 2 while the second cluster comprises sites 3, 4 and 5. For the purpose of this example, we have chosen a population where clusters are easily identifiable by looking at the connectivity matrix, but in most cases the identification is not straightforward. The eigenvalues of this matrix are [1.775, 1.464, -0.677, 0.601, -0.185]; the right eigenvector $\mathbf{u_{max}}$ associated with the dominant eigenvalue (λ_{max} =1.775) is: [0.004, 0.003, 0.463, 0.655, 0.596] and

the left eigenvector $\mathbf{v_{max}}$ is [-0.003, 0.002, 0.598, 0.648, 0.472]. The donor-recipient product $\mathbf{u_{max}v_{max}}$ is [10^{-5}, 10^{-5}, 0.277, 0.425, 0.281]. These values show that population growth is dominated by the second cluster. If two sites were to be chosen for protection, these would be sites 4 and 5 (**Figure A1(b)**). However, this choice would leave the first cluster unprotected and is spatially unbalanced. This result is due to the higher connectivity in the second cluster relative to the first. It is desirable to find a solution that protects demes in both clusters. To achieve this, the two clusters can be considered as two independent matrices as in **Table A2**.

The two matrices in **Table A1** were formed by taking the connections within each cluster and disregarding the between-cluster connections. As between-cluster connections are very weak, there is very little loss of information in doing this. This can be seen on the eigenvalues of the two matrices. The dominant eigenvalues are $\lambda^{(1)}_{max}$ =1.464 for the first matrix and $\lambda^{(2)}_{max}$ =1.775 for the second matrix. Note that $\lambda^{(1)}_{max}$ and $\lambda^{(2)}_{max}$ are equal respectively to the second-dominant and the dominant eigenvalue of the full matrix. The right and left eigenvectors of the first matrix are $\mathbf{u_{max}}$ = [0.781, 0.624] and $\mathbf{v_{max}}$ = [0.800, 0.600], and the donor-recipient values are $\mathbf{v_{max}u_{max}}$= [0.625, 0.375]: on the basis of these values, we would choose deme 1 for protection in the first cluster. For the second matrix, we calculate $\mathbf{u_{max}}$ = [0.463, 0.656, 0.596], $\mathbf{v_{max}}$ = [0.597, 0.648, 0.471] and $\mathbf{v_{max}u_{max}}$= [0.277, 0.425, 0.281]; thus, we would choose deme 4 for protection and end up with a protection plan as in **Figure A1(c)**, which is spatially balanced and preferable to the unbalanced one. This solution allows for persistence of more sites than in the case of the full matrix, because unprotected sites benefit from propagule supply from protected sites. In the full matrix case, site 3 can benefit from propagule supply from site 4 and 5, but sites 1 and 2 remains completely isolated. Conversely, choosing sites 1 and 4 for protection allows for downstream effects on all other unprotected sites. Even if sites 1 and 4 are isolated from one another, they can harbor self-sustaining populations if there is enough local retention. Our approach allows for taking into account the effects of connectivity on persistence using a quantitative metric, the metapopulation growth rate, which is explicitly maximized by our algorithm.

Note that the elements of the eigenvectors of the second matrix are similar to their corresponding ones in the full matrix. However, this is not true for the eigenvectors of the first matrix, which were “obscured” by the much higher connectivity of the second cluster in the full matrix. Splitting the matrix, therefore, allowed us to identify the highest contributing sites to population growth in both clusters.

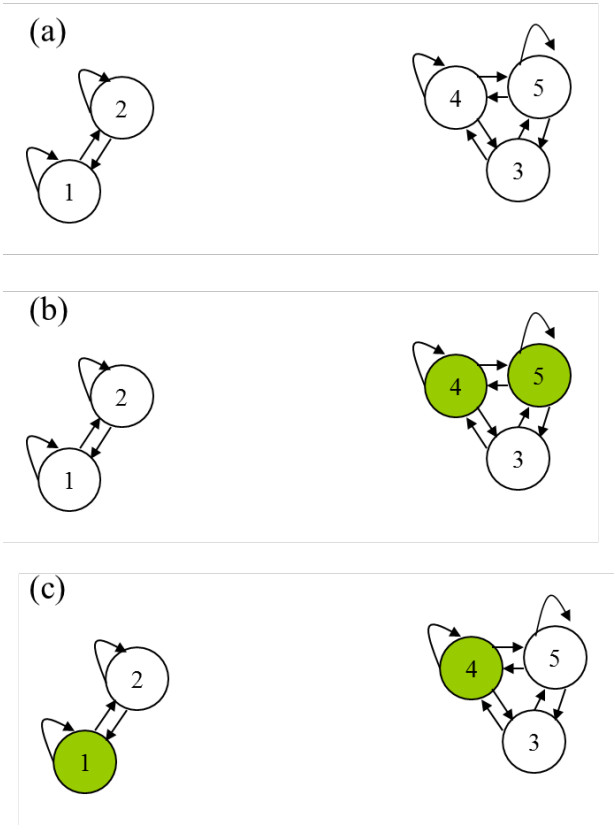

Figure A1. (a) Example of a population with two nearly independent clusters. Strong connections are represented with arrows, weak connections are not plotted for clarity. (b) Protection plan based on the analysis of the full connectivity matrix. (c) Protection plan based on the analysis of two connectivity matrices, one for each cluster, obtained by splitting the full matrix. In (b) and (c), green indicates the sites chosen for protection.

Table A1. Connectivity matrix relative to the population pictured in Figure A1

	Site 1	*Site 2*	*Site 3*	*Site 4*	*Site 5*
Site 1	0.846	0.773	0.000	0.001	0.001
Site 2	0.825	0.433	0.000	0.001	0.001
Site 3	0.001	0.000	0.016	0.833	0.452
Site 4	0.001	0.000	0.989	0.839	0.261
Site 5	0.001	0.000	0.870	0.231	0.844

Table A2. Connectivity matrices for the two clusters of demes. Values are taken from the matrix in Table A1. Note that in this formulation the weak connections between clusters are lost.

	Site 1	*Site 2*
Site 1	0.846	0.773
Site 2	0.825	0.433

	Site 3	*Site 4*	*Site 5*
Site 3	0.016	0.833	0.452
Site 4	0.989	0.839	0.261
Site 5	0.870	0.231	0.844

Literature cited

Nilsson Jacobi, M. and Jonsson, P. R. 2011. Optimal networks of nature reserves can be found through eigenvalue perturbation theory of the connectivity matrix. — Ecological Applications 21: 1861-1870.

Appendix 2

Three-dimensional sea current velocities were calculated with the NEMOMED12 model (Beuvier et al. 2012a, Beuvier et al. 2012b), a Mediterranean Sea regional configuration of the ocean general circulation model NEMO (Madec 2008). The model has a horizontal resolution of $1/12^{th}$ degree, corresponding to a 6-8 km horizontal cell width. We thus consider this model as eddy-resolving, even if it might be too coarse to resolve small-scale circulation, particularly around complex topographical features such as headlands and semi-enclosed bays (Largier 2003). The model has 50 vertical layers, unevenly spaced from 1 m-thick at the surface to 450 m-thick at the bottom, with 35 levels in the first 1000 m. The model was forced with the atmospheric wind stress, total and solar heat fluxes, total freshwater flux (evaporation minus precipitation), and river discharge (33 main rivers mouths plus a coastal runoff) coming from the ARPERA dataset (Herrmann and Somot 2008). NEMOMED12 returns the three-dimensional velocity, potential temperature, salinity and water potential density fields, and the sea surface elevation, from October 1st 1998 to December 31st 2008. As far as surface circulation is concerned, comparisons with altimetry products indicate that NEMOMED12 reproduces the observed circulation patterns in the Mediterranean (Beuvier 2011) as well as high eddy activities at meso-scale (Beuvier et al. 2012a). Further details on NemoMed12 can be found in (Andrello et al. 2013).

Daily outputs of zonal and meridional velocities from NEMOMED12 were used in this study to simulate passive larval dispersion using the software Ichthyop 3.1 (Lett et al. 2008). As the tidal signal in the Mediterranean is relatively small, daily currents were considered appropriate inputs to Ichthyop. In the simulation, we released larvae in packs of one thousand every three days from the July 1^{st} day until the July 28^{th} day (ten release events). To smooth inter-annual variability due to sea currents, we pooled the larval dispersal simulations for years 2004 to 2008. Thus, over the five years, we used 50,000 larvae per planning units. This allowed us to detect connection probabilities as small as 0.00002. Larvae were released near the sea surface (20 cm depth). Horizontal diffusion

was applied via a random walk for individual larvae to account for sub-grid-scale hydrodynamics associated with coastal features (reefs, bays, gulfs, etc.) following Peliz et al. (2007). Planktonic larval duration (PLD) was set to 30 days. Larvae were subject to sea currents only (passive dispersal) without simulating active swimming or vertical migration. Previous analysis showed that vertical migration reduces connectivity (Andrello et al. 2013).

Literature cited

Andrello, M. et al. 2013. Low Connectivity between Mediterranean Marine Protected Areas: A Biophysical Modeling Approach for the Dusky Grouper *Epinephelus marginatus*. — PLoS ONE 8: e68564.

Beuvier, J. 2011. Modelling the long-term variability of circulation and water masses in the Mediteranean Sea: impacts of the ocean-atmosphere exchanges. Mechanics department. PhD Thesis. Ecole Polytechnique, Palaiseau, France, p 290.

Beuvier, J. et al. 2012a. Spreading of the Western Mediterranean Deep Water after winter 2005: time-scales and deep cyclone transport. — Journal of Geophysical Research 117: C07022.

Beuvier, J. et al. 2012b. MED12, oceanic component for the modeling of the regional Mediterannean Earth system. — Mercator Ocean Quarterly Newsletter 46: 60-66.

Herrmann, M. J. and Somot, S. 2008. Relevance of ERA40 dynamical downscaling for modeling deep convection in the Mediterranean Sea. — Geophysical Research Letters 35: L04607.

Largier, J. 2003. Considerations in Estimating Larval Dispersal Distances from Oceanographic Data. — Ecological Applications 13: S71-S89.

Lett, C. et al. 2008. A Lagrangian tool for modelling ichthyoplankton dynamics. — Environmental Modelling & Software 23: 1210-1214.

Madec, G., and the Nemo team 2008. NEMO ocean engine. Note du Pôle de modélisation. Institut Pierre-Simon Laplace (IPSL), France.

Peliz, A. et al. 2007. A study of crab larvae dispersal on the Western Iberian Shelf: Physical processes. — Journal of Marine Systems 68: 215-236.